Korean J. Chem. Eng., 36(11), 1814-1825 (2019)
DOI: 10.1007/s11814-019-0367-y

pISSN: 0256-1115
eISSN: 1975-7220

Development of magnetically separable Cu catalyst supported by pre-treated steel slag

Sunho Yoon and Sungjun Bae†

Department of Civil and Environmental Engineering, Konkuk University,
120 Neungdong-ro, Gwangjin-gu, Seoul 05029, Korea
(*Received 30 June 2019 • accepted 15 August 2019*)

Abstract−Wastewater contaminated with organic compounds is a serious problem; therefore, many catalysts, especially copper catalysts, have been developed to treat it and remove contaminants before discharge. However, such separation and reuse of these catalysts is often challenging. Steel slag (SS), a by-product of steel production, is produced in large quantities and requires careful disposal. Therefore, in this study, we developed a magnetically recyclable copper catalyst utilizing pre-treated magnetic steel slag (MSS) as a support. First, magnetic separation was carried out to remove calcium silicate impurities such as alite and belite in MSS up to five times, thus increasing the Fe content of the MSS. We synthesized the Cu catalyst supported by MSS (donated as Cu@MSS) and characterized the catalyst by various surface analysis techniques, showing the presence of CuO and $CuCO_3$ nanoparticles on the MSS surface. In catalytic reduction tests of *para*-nitrophenol using sodium borohydride in the presence of Cu@MSS, the reaction was accelerated when using the five-times pre-treated MSS because of the removal of inhibitors such as calcium compounds, as well as the high content of iron oxides leading to a synergetic effect with metallic Cu in this study. In addition, we investigated the effects of various factors, including Cu loading, sodium borohydride concentration, and catalyst dosage, on the catalytic activity of Cu@MSS. The catalyst was found to be stable and reusable. In summary, these results suggest that treated SS can be used as a support material for copper catalysts for the treatment of contaminated wastewater and the easy separation and reuse of the catalyst.

Keywords: Steel Slag, Magnetic Separation, Cu Catalyst, *p*-Nitrophenol, Recycling

INTRODUCTION

The agricultural and industrial revolutions have increased the world population dramatically, which has resulted in many global environmental issues (e.g., air, water, and land pollution). Furthermore, the generation and disposal of solid waste have become significant problems, especially in urban areas, which has resulted in increased environmental regulation related to the management of solid waste [1,2]. Most solid waste is dumped in landfill sites as a final disposal method, but these sites have a maximum capacity, and many of these sites will close in the near future [3,4]. Thus, the recycling of the solid waste has attracted attention because of increased awareness and interest in sustainable development [5,6].

Steel slag (SS) is generated from steel plants during the conversion of iron ore to steel products and is generated in large quantities from industrial facilities [4,5,7]. More than one-billion tons of steel are produced annually worldwide [8], and approximately 400 kg of solid waste can be generated when one ton of steel is produced [4]. Blast furnace slag (BFS) and SS are the two main solid waste products of the iron-making and steel-making processes, respectively [8]. Currently, BFS is recycled to form valuable products (i.e., granulated slag and partial Portland cement) in many countries owing to its numerous advantages (e.g., relatively homogeneous particles and the increase in long-term strength and durability of the microstructure of hardened Portland cement) [5,8,9]. In contrast to BFS, SS cannot be upcycled easily, and it is mostly used as a simple aggregate because it has a relatively low hydraulicity and volumetric expansion caused by free CaO [8,9]. Therefore, the development of upcycling methods for SS that would allow its application in industrial and environmental fields with high efficiency is required.

Many suggestions for the reuse SS in value-added ways have been proposed, for example, in CO_2 sequestration [10], as a fertilizer [7,11], or as a soil stabilizer [7,12]. Recently, SS has been used in wastewater treatment processes as an adsorbent and catalyst [13-15]. Among these applications, its use as an environmental catalyst could be the most value-added method because SS typically contains various metal oxides (e.g., Fe_2O_3, SiO_2, MnO, and Al_2O_3) [16-18] that could react with wastewater pollutants directly or be used as the supporting material for the development of other reactive catalysts [15,18,19]. In general, a variety of support materials, such as silica oxides, carbon materials, membranes, and zeolites, are used to maintain the dispersibility of metallic catalysts, resulting in enhanced catalytic reactivity [6,20-22]. However, these support materials require time-consuming processes such as centrifugation or filtration for purification [18,19,23].

Normally, the weight percentage of iron oxides in SS is greater than 20%, and these oxides are a mixture of magnetic minerals (i.e., magnetite (Fe_3O_4) and maghemite (γ-Fe_2O_3)) and wüstite (FeO) [4,15]. Magnetite and maghemite are well known as insoluble and superparamagnetic materials [23], meaning that some parts of SS can be used as a magnetically separable support material for the

†To whom correspondence should be addressed.
E-mail: bsj1003@konkuk.ac.kr

development of reactive environmental catalysts. Indeed, many researchers have used magnetic particles as a support material for the development of magnetically separable catalysts [20,23,24]. However, to date, there has been limited research into the possibility of using SS for the development of magnetically separable metal catalysts.

In this study, we developed magnetically separable catalysts using pre-treated SS. Copper was selected as a catalytic metal because it can replace other precious metals such as Au, Ag, Pd, and Pt with a lower cost and high reusability [25]. In addition, Cu nanoparticles show excellent performance in the catalytic reduction of organic pollutants compared to those of other first-row transition metals [26]. Therefore, the objectives of this study were to i) investigate the physical and chemical changes of SS before and after the pretreatment (i.e., magnetic separation and washing process), ii) evaluate the catalytic activity of SS itself after the successive magnetic separation processes, iii) investigate the surface characteristics of the developed Cu catalyst supported by magnetically separable SS (MSS) using various surface analysis techniques, iv) evaluate the effects of experimental factors (Cu loading, catalyst concentration, and reductant (i.e., $NaBH_4$) concentration), and v) demonstrate the reusability of the developed catalysts for the treatment of wastewater containing organic pollutants. We selected *para*-nitrophenol (*p*-NP) as a target nitroaromatic toxic pollutant in wastewater, and this is reduced to *para*-aminophenol (*p*-AP) by catalytic reduction with $NaBH_4$ [18-20,27].

MATERIALS AND METHODS

1. Materials and Chemicals

The SS was obtained from a steel product company in South Korea. Other chemicals such as *p*-nitrophenol (≥99%) and sodium borohydride (≥99%) were purchased from Sigma-Aldrich. Copper sulfate pentahydrate (99%, Samchun Chemical Co. Ltd., South Korea) was used for the preparation of the Cu precursor solution. The solutions used in all experiments were prepared using deionized water (DIW, 18.2 MΩ) purified using an ultrapure water filtration system (HUMAN POWER I+, Human Corp., South Korea).

2. Preparation of Fine Raw Steel Slag

SS having particle sizes of 3-5 cm (Fig. 1(a)) was crushed using a hammer mill system to obtain millimeter-sized SS (Fig. 1(b)). Then, 500 g of crushed SS was subjected to secondary crushing by using a ball mill system at 35 rpm for 30 min. The SS after the secondary crushing was sieved to obtain fine SS having a particle size of less than 106 μm (Fig. 1(c)). Unless otherwise stated, the fine SS after the sieving process is defined as raw SS (RSS) in this paper.

3. Preparation of Cu-MSS Catalysts

To separate the magnetic and non-magnetic fractions of RSS, the RSS was transferred to a glass beaker containing DIW to prepare the RSS suspension (20 g/L). A neodymium magnet was placed on the outside of beaker and the suspension was mechanically stirred at 300 rpm for 2 h. After the stirring was stopped, the non-magnetic RSS was allowed to settle for 1 h, and the MSS attached to the walls of the flask was collected. The collected MSS and non-magnetic RSS (NMSS) were centrifuged (5,000 rpm, 3 min) and dried in an oven at 105 °C overnight. To obtain high-purity MSS, we repeated this procedure up to five times. The wastewater after the purification step was filtered through a 0.2-μm membrane filter (Whatman), and the pH of the solution and leaching of Ca^{2+} were determined at each step.

The Cu-doped catalysts were prepared through an impregnation method. An exact amount (0.1 g) of RSS and three different MSSs (i.e., 1 (1^{st}-MSS), 3 (3^{rd}-MSS), and 5-times (5^{th}-MSS) purified MSS) were mixed with 10 mL DIW for 10 min before the addition of the Cu precursor. Then, the Cu precursor solution (0.25-1.5 wt%) was introduced into the support suspensions and they were mixed (700 rpm) for 2 h. The mixed suspension was dried in an oven at 105 °C overnight and then calcined at 350 °C (2 h) to stabilize the Cu nanoparticles on the surface of the supports.

4. Batch Experiments for *p*-NP Reduction

The catalytic activity of the prepared Cu catalysts was investigated using *p*-NP reduction experiments with $NaBH_4$ under ambient conditions. The prepared catalysts were transferred to a quartz cuvette (10-mm path length), and 1.9 mL DIW and 0.1 mL *p*-NP (3 mM) were added to the quartz cuvette sequentially. Finally, the catalytic reaction was initiated by adding 1 mL of freshly prepared $NaBH_4$ stock solution, yielding a 0.1 mM initial *p*-NP concentration. For parametric studies, different concentrations of Cu (0.25-1.5 wt%), catalyst (1-3.33 g/L), and $NaBH_4$ (10-100 mM) were used.

For recycling tests, the *p*-NP (0.1 mM) reduction was carried out in $NaBH_4$ (25 mM) solution using 2 g/L of 1 wt% Cu doped catalyst (i.e., Cu@MSS). After finishing the reaction, the catalyst used was magnetically collected at the bottom of the cuvette, and 2.5 mL of the supernatant was discarded. Then, 2.5 mL of pure DIW was used to wash out the remained *p*-AP and $NaBH_4$ from the inside of the cuvette. This washing procedure was repeated three times. Finally, 1.4 mL of DIW and 0.1 mL of *p*-NP (3 mM) were introduced to the cuvette, and then, 1 mL of $NaBH_4$ (75 mM) was added to the

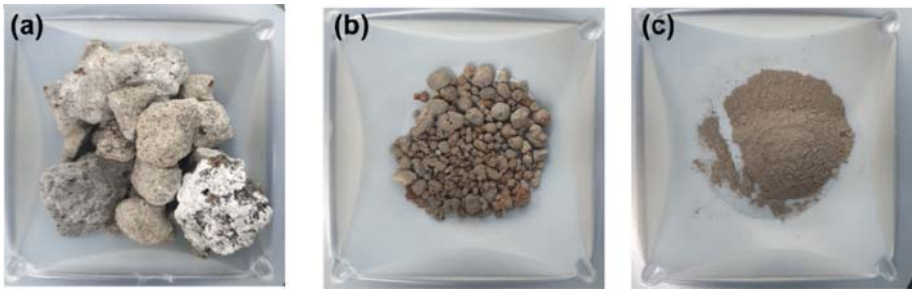

Fig. 1. Photo images of initial SS (a) before and (b) after crushing by hammer mill and (c) after crushing by ball mill.

quartz cuvette for the next recycling test.

5. Analytical Methods

Aqueous samples were collected at each step after magnetic separation for Ca^{2+} ion determination by ion chromatography (IC) (883 Basic IC Plus, Metrohm, Switzerland) equipped with a compact auto-sampler (863 Compact IC, Metrohm, Switzerland) and cation column (Metrosep C4-150/4.0, Metrohm, Switzerland). In addition, the chemical composition of the SS was determined by X-ray fluorescence (XRF, PANalytical, Epsilon 3-XL, Germany). The crystalline characteristics of RSS, NMSS, MSS, and Cu@MSS were analyzed by X-ray diffraction (XRD) (Rigaku, Japan) equipped a HyPix-3000 detector at scan speed of 3^{o} min^{-1}. Morphological characteristics were identified by high-resolution field-emission scanning electron microscopy (HR-SEM) (Hitachi, Japan) equipped with an energy-dispersive X-ray spectroscopy (EDS). The samples were loaded on a carbon tape and coated by platinum for 30 s [28]. X-ray photoelectron spectroscopy (XPS) analysis was carried out to identify the oxidation state of Cu on the surface of Cu@MSS using a Sigma Probe system (Al source $K\alpha$ X-rays, 1,486.7 eV, Thermo Fisher Scientific, USA). Surface charging effects were corrected with respect to the C 1s peak at 284.8 eV as a reference. The conversion from *p*-NP to *p*-AP during the catalytic reaction was measured by UV-vis spectrophotometer (Agilent 8453, Agilent, USA) at wavelengths of 400 and 300 nm, respectively.

RESULTS AND DISCUSSION

1. Variation in the Chemical Composition in RSS and MSSs

The morphological and elemental features of the RSS were investigated by HR-FESEM at different magnifications (Fig. 2). Overall, the RSS particles had a non-uniform size and shape after the physical crushing processes (Fig. 2(a)). In addition, we observed small nanoparticles on the surface of RSS in the enlarged images (Fig. 2(b)), possibly calcium oxides, which are often observed in other solid waste materials (e.g., fly ash) containing Fe, Si, Al, and Ca [18,19]. The results of EDS mapping (Fig. 2(c)) show that the RSS

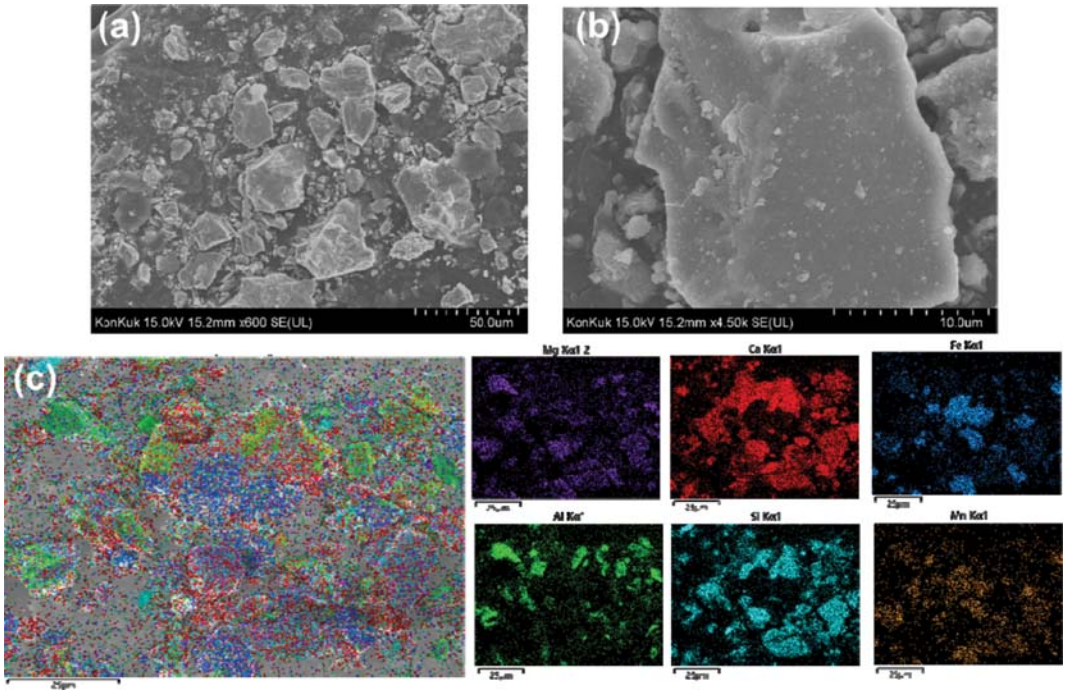

Fig. 2. SEM images of (a) RSS and (b) the enlarged image. (c) EDS analysis of RSS and their results showing the electron mapping of Mg, Ca, Fe, Al, Si, and Mn.

Table 1. XRF results for RSS, NMSS, and MSSs

Component	RSS (wt%)	NMSS (wt%)	1st MSS (wt%)	2nd MSS (wt%)	3rd MSS (wt%)	4th MSS (wt%)	5th MSS (wt%)	Remark
CaO	31.2	43.7	26.9	22.4	19.9	18.3	17.7	Decrease
Fe_2O_3	31.8	16.6	38.1	44.5	50.5	51.4	52.3	Increase
SiO_2	14.1	18.0	12.2	9.9	7.7	7.8	7.5	Decrease
Al_2O_3	7.1	7.4	6.4	5.8	4.6	4.7	4.5	Decrease
MnO	8.4	5.9	9.4	10.4	10.6	11.1	11.1	Increase
MgO	3.7	3.8	3.6	3.4	3.1	3.3	3.4	-
Cr_2O_3	2.0	2.2	2.0	2.0	1.8	1.8	1.6	-
Etc	1.7	2.4	1.4	1.6	1.8	1.6	1.9	-

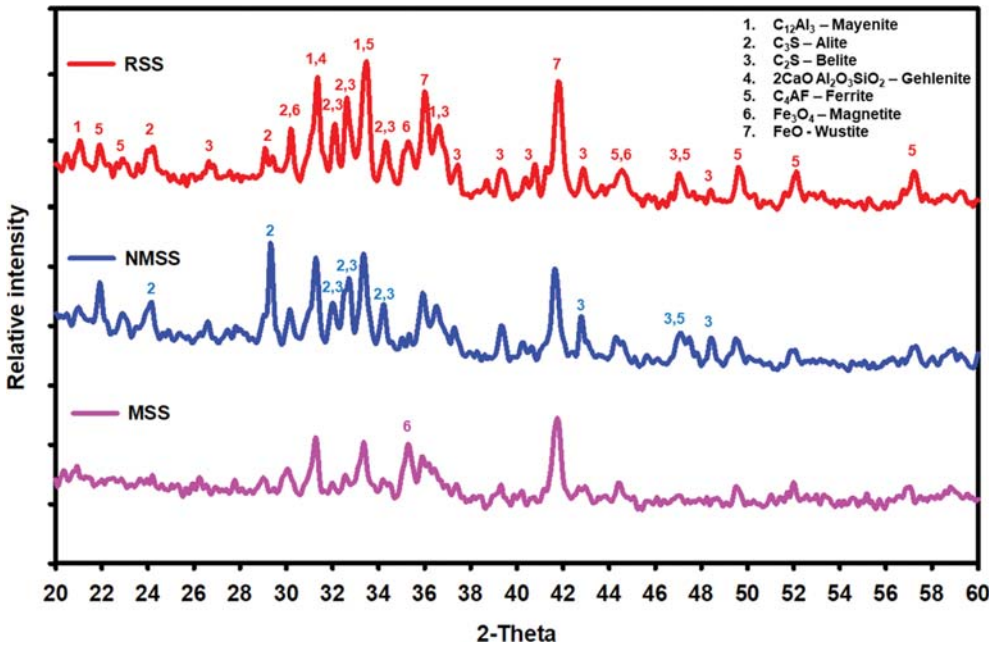

Fig. 3. XRD patterns of RSS, NMSS, and 5th-MSS.

particles contained different elements such as Mg, Ca, Fe, Al, Si, and Mn.

Table 1 shows the results of XRF analysis for RSS and different MSSs. The RSS was composed of mostly Fe_2O_3 (31.8%) and CaO (31.2%), followed by other minor mineral phases such as SiO_2 (14.1%), MnO (8.4%), Al_2O_3 (7.1%), MgO (3.7%), Cr_2O_3 (2.0%), and others (1.7%). As the number of magnetic separations increased, the content of Fe_2O_3 increased significantly (31.8%→52.3%), but a decrease in CaO (from 31.2→17.7%), SiO_2 (14.1→7.5%), and Al_2O_3 (7.1→4.5%) was observed. Compared to the MSS, the NMSS, which settled during magnetic separation, contained high content of CaO (43.7%) and SiO_2 (18.0%) with relatively low content of Fe_2O_3 (16.6%) and MnO (5.9%).

Fig. 3 shows the XRD diffractograms of RSS, NMSS, and 5th-MSS, which revealed that calcium, aluminum, silica, and iron were present in RSS in the form of various complex minerals such as wüstite, gehlenite, magnetite, mayenite, alite, belite, and ferrite. This is consistent with a typical XRD result of RSS [5,17,29]. Interestingly, we observed no significant peaks corresponding to alite (Ca_3Si) and belite (Ca_2Si) in the MSS sample compared to that of NMSS. Furthermore, peaks corresponding to magnetite/maghemite were only detected in the MSS sample not in the NMSS sample. The XRF and XRD results indicate that 1) the magnetic properties were derived from magnetite/maghemite likely crystal structure and 2) Ca_3Si and Ca_2Si present on the surface of NMSS can be removed easily during the magnetic separation with water. Based on the XRF results, which show increases in both Fe and Mn, we can suggest that the main Fe form of MSS is manganese ferrite ($MnFe_2O_4$), which has a similar XRD pattern to those of pure magnetite/maghemite [30,31].

To confirm the leaching of Ca oxides during the preparation of MSS, we measured the pH and Ca^{2+} concentration in each solution used for the magnetic separation (Fig. 4). After the first separation, the pH increased from 5.7 to around 11, and the pH decreased continuously as the separation was repeated (around to pH 8 after in the 5th-MSS). Furthermore, the concentration of Ca^{2+} leaching from the RSS suspension (from 80 mg/L) decreased continuously and reached 20 mg/L in the 5th-MSS. The increase in pH and decrease in Ca^{2+} concentration with increasing number of separations could be caused by the dissolution of water-soluble calcium materials (e.g., alite and belite) [18]. Alite and belite are the main components of Portland cement and could have reacted with water as shown in Eqs. (1) and (2).

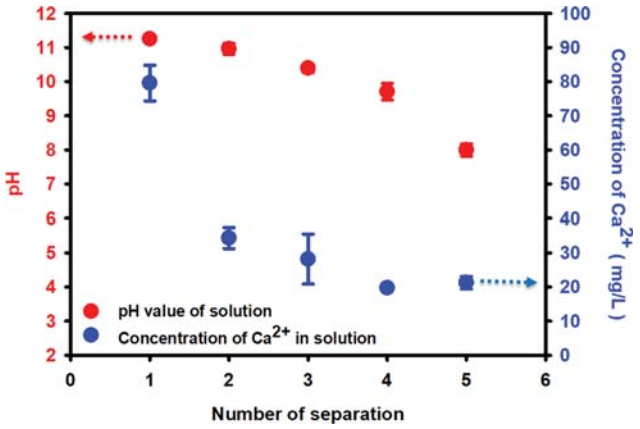

Fig. 4. Variation of pH and Ca^{2+} concentration as increasing the number of magnetic separation. Experimental condition: [RSS]= 20 g/L.

$$\text{Alite: } 2Ca_3SiO_5+6H_2O \rightarrow 3CaO\cdot 2SiO_2\cdot 3H_2O+3Ca(OH)_2 \quad (1)$$

$$\text{Belite: } 2Ca_2SiO_4+4H_2O \rightarrow 3CaO\cdot 2SiO_2\cdot 3H_2O+Ca(OH)_2 \quad (2)$$

Calcium hydroxide produced by reactions 1 and 2 is also slightly

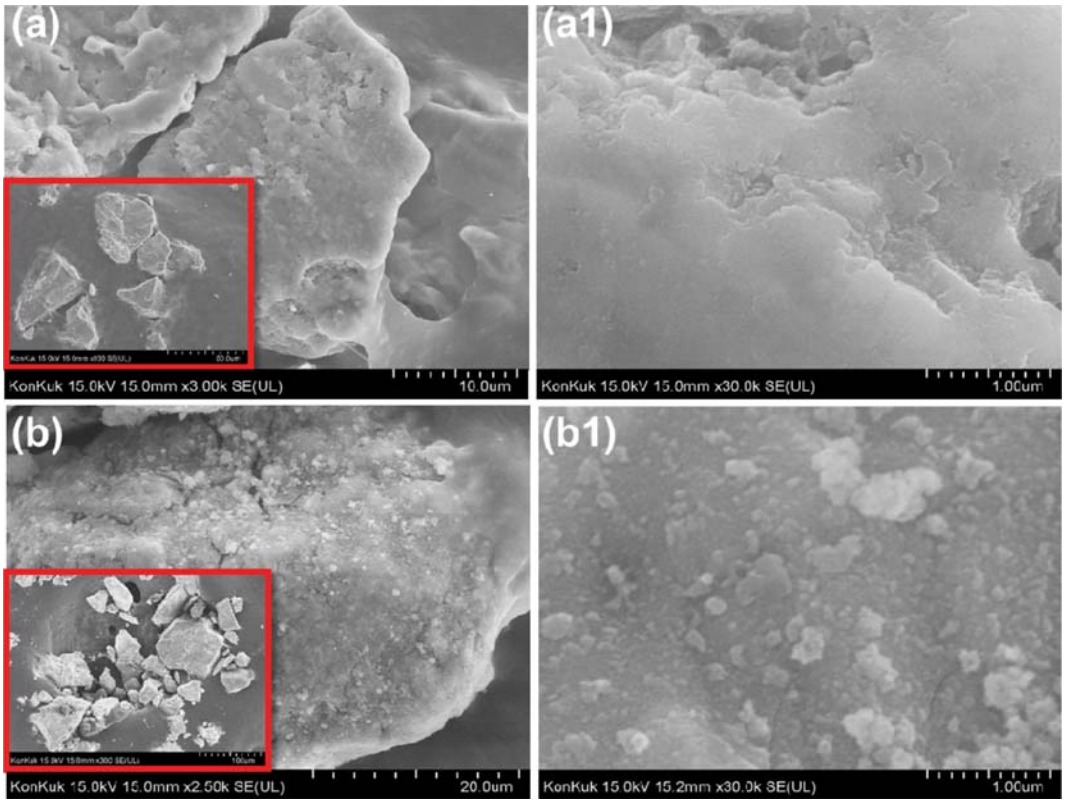

Fig. 5. SEM images of (a and a1) 5th-MSS and (b and b1) 1 wt% Cu@MSS.

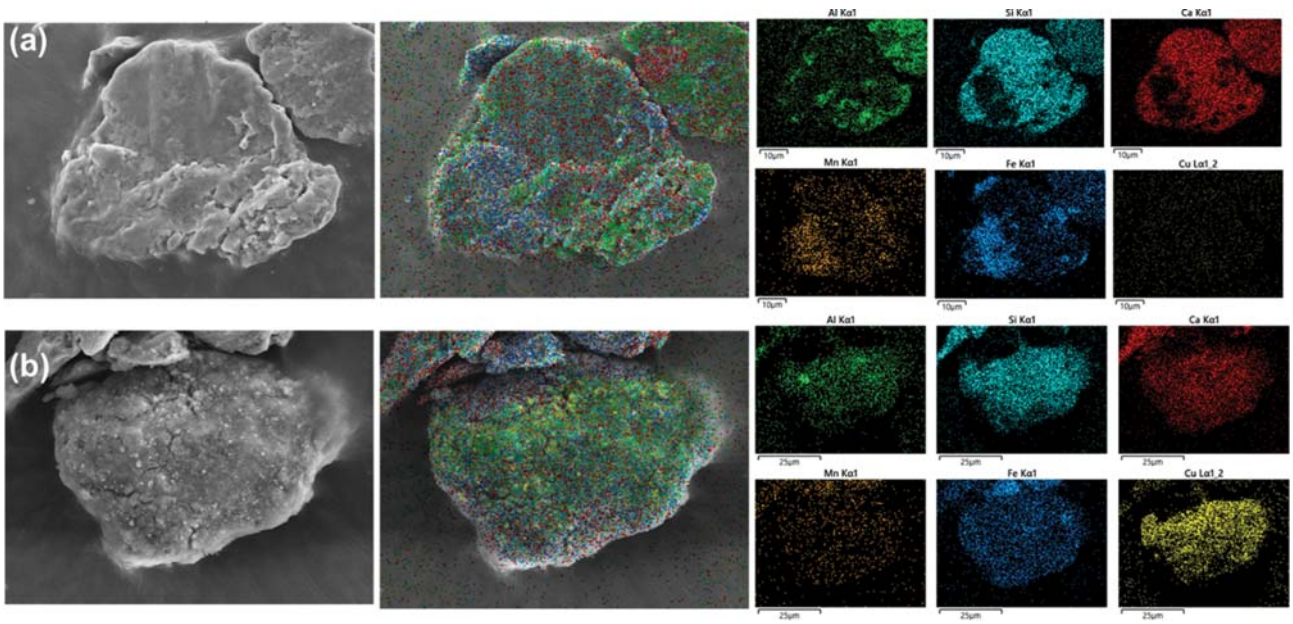

Fig. 6. EDS analysis of (a) MSS and (b) Cu@MSS.

soluble in water (K_{sp}=5.5×10^{-6}), which causes an increase in the solution pH after the first separation process ($Ca(OH)_2 \rightarrow Ca^{2+} + 2OH^-$). However, a significant amount of alite and belite could be washed out on the surface of MSS during the repeated separation steps, which reduces the impact of Ca dissolution (i.e., increase in pH and leaching of Ca^{2+}).

2. Characterization of Cu@MSS

The morphological characteristics of MSS (5th) and Cu@MSS were investigated by HR-FESEM (Fig. 5). Fig. 5(a) shows the surface image of MSS after the fifth separation process. In particular, the enlarged image of MSS (Fig. 5(a1)) shows a relatively clean surface compared to the initial RSS surface (Fig. 2(b)). This result

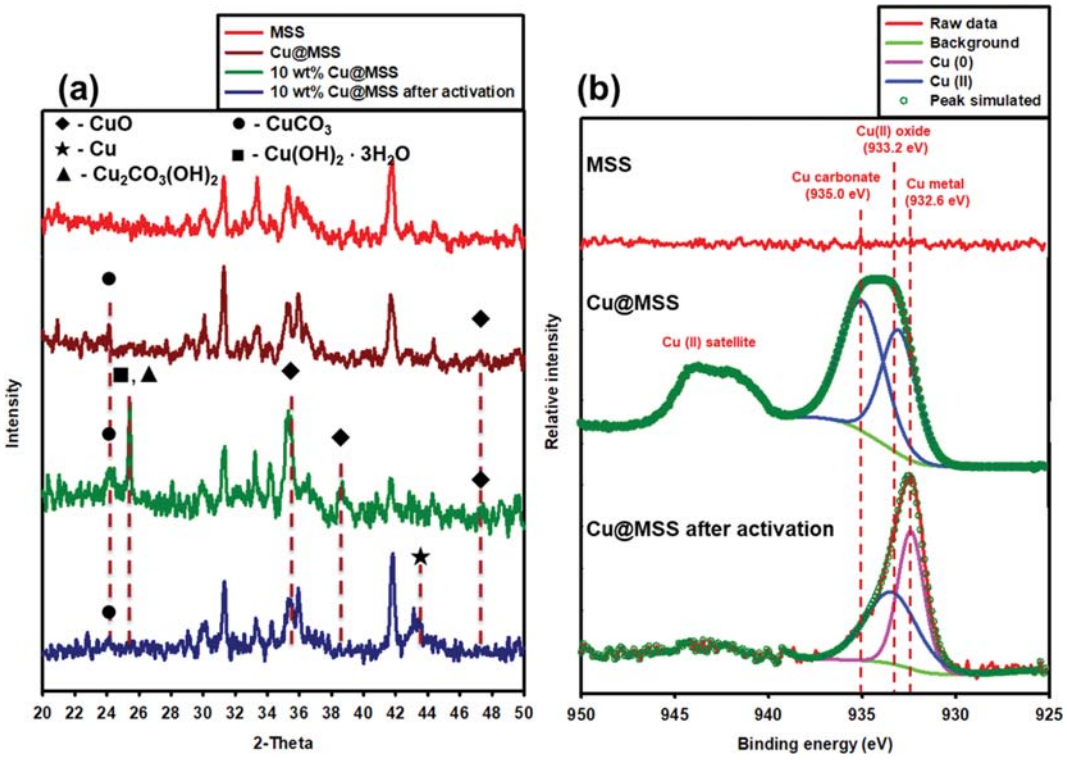

Fig. 7. (a) XRD patterns of MSS, 1 wt% Cu@MSS, 10 wt% Cu@MSS, and 10 wt% Cu@MSS after the activation by $NaBH_4$ solution (25 mM), (b) XPS spectra for the narrow scan of Cu($2p_{3/2}$) on the surface of MSS, 1 wt% Cu@MSS, and 1 wt% Cu@MSS after the activation by $NaBH_4$ solution (25 mM).

clearly indicates that the water-soluble calcium oxides present on the RSS surface were removed by hydrolysis reactions with water during the aqueous magnetic separation. In contrast, we observed a significant change in the surface morphology in Cu@MSS (Fig. 5(b)); crucially, we observed nanoparticles on the surface of MSS (Fig. 5(b1)). The results of EDS mapping (Fig. 6(a)) confirmed that Al, Si, Ca, Mn, and Fe were the major components in MSS without Cu, whereas a significant amount of Cu was well distributed on the surface of Cu@MSS (Fig. 6(b)). The results show that Cu nanoparticles had been successfully doped on the surfaces of the MSS particles.

Fig. 7(a) shows the XRD patterns of MSS and Cu@MSS (1 and 10 wt% Cu loadings). Furthermore, 10 wt% Cu@MSS activated by $NaBH_4$ solution was also analyzed because the model reaction was tested in $NaBH_4$ suspension. The peaks associated with Cu were not observed in the MSS and 1 wt% Cu@MSS samples because of the low Cu contents, which were near the detection limit of the XRD analysis [32]. When we increased the Cu loading to 10 wt%, the XRD pattern of Cu@MSS contained three clear peaks at Bragg angles (2θ) of 35.6°, 38.7°, and 48.6°, indicating the existence of CuO particles (JCPDS card # 48-1548) on the MSS surface [33]. In addition, we observed an increase in the intensity of the peak at around 25°, which corresponded to copper carbonate and hydroxycarbonate complexes [34-36]. After the catalyst activation, the peaks corresponding to CuO and Cu complexes decreased significantly and a new peak appeared at 43.5°, which was assigned to metallic copper (JCPDS card # 04-0836) [37].

Fig. 7(b) shows the narrow scan XPS results (950-925 eV) of Cu($2p_{3/2}$). No Cu peak was detected on the MSS surface, whereas two broad Cu(II) peaks at 945-940 eV (Cu(II) satellite peak) and 939-930 eV were observed for the Cu@MSS. Furthermore, we observed two distinct peaks corresponding to CuO (933.2 eV) and $Cu_2CO_3(OH)_2$ (935.0 eV) between 939-930 eV [25,38]. After activation, we observed the disappearance of the Cu (II) satellite peak and shift of main peak of Cu($2p_{3/2}$) to a lower binding energy of 932.6 eV, which was assigned to the metallic copper. These results are in good agreement with the XRD results, indicating that Cu(II) doped on the MSS surface could be reduced to metallic copper (i.e., Cu(0)) particles by $NaBH_4$ ($2Cu^{2+}+BH_4^-+3H_2O \rightarrow 2Cu+B(OH)_3+2H_2+3H^+$), thus possessing the potential to act as a catalyst for the reduction of *p*-NP, as discussed in the next section.

3. Enhanced *p*-NP Reduction by the Cu@MSS Catalyst with $NaBH_4$

Fig. 8(a) shows the general UV-vis spectra of *p*-NP under different pH conditions. Under acidic conditions (pH 2.5), a strong absorbance peak was found for *p*-NP at 317 nm. However, the absorbance peak was shifted to 400 nm (*p*-nitrophenolate ion) as the pH increased because of the deprotonation of *p*-NP (pK_a=7.16) [18,39]. In this study, all the experiments were conducted under alkaline conditions (>pH 10) because of the use of an $NaBH_4$ solution [19,20,27]. Therefore, the concentration of *p*-NP was calculated from the absorption of the *p*-nitrophenolate ion at 400 nm.

The Cu@MSS suspension in the absence of $NaBH_4$ (Fig. 8(b)) showed the conversion of *p*-NP to the *p*-nitrophenolate ion over a

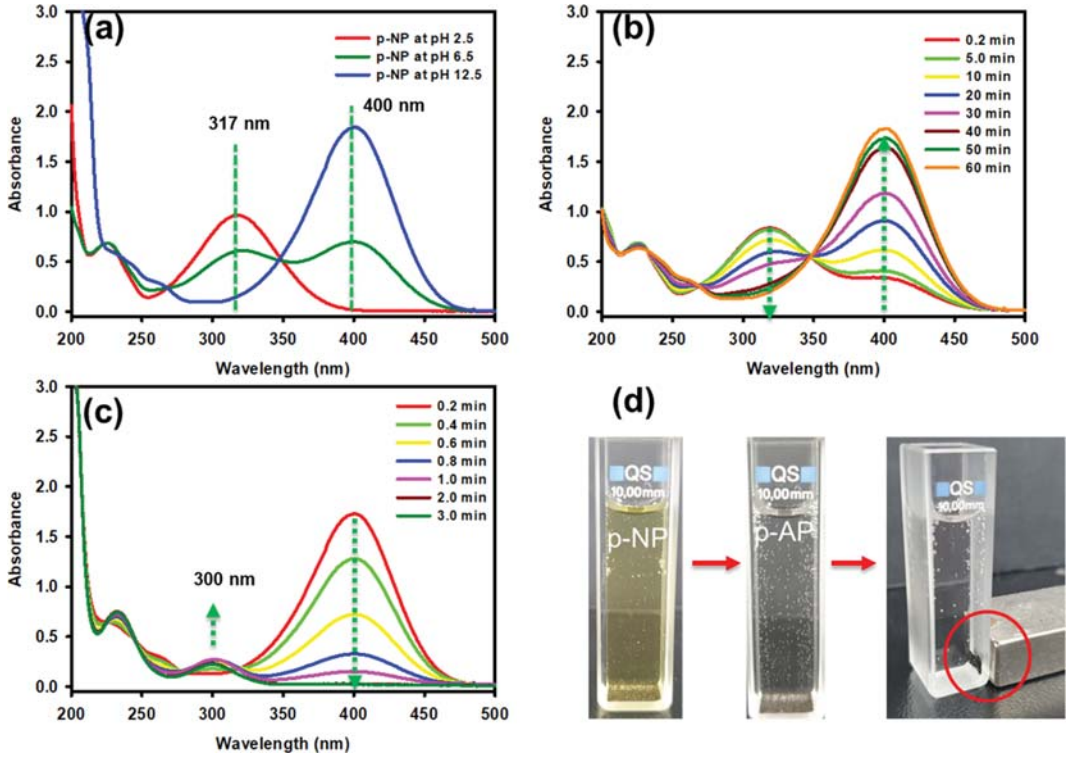

Fig. 8. UV-vis spectra of *p*-NP (0.1 mM) (a) at different pHs (b) during the reaction by Cu@MSS without $NaBH_4$, and (C) with $NaBH_4$ (25 mM). (d) Color change of *p*-NP suspension during the catalytic reaction.

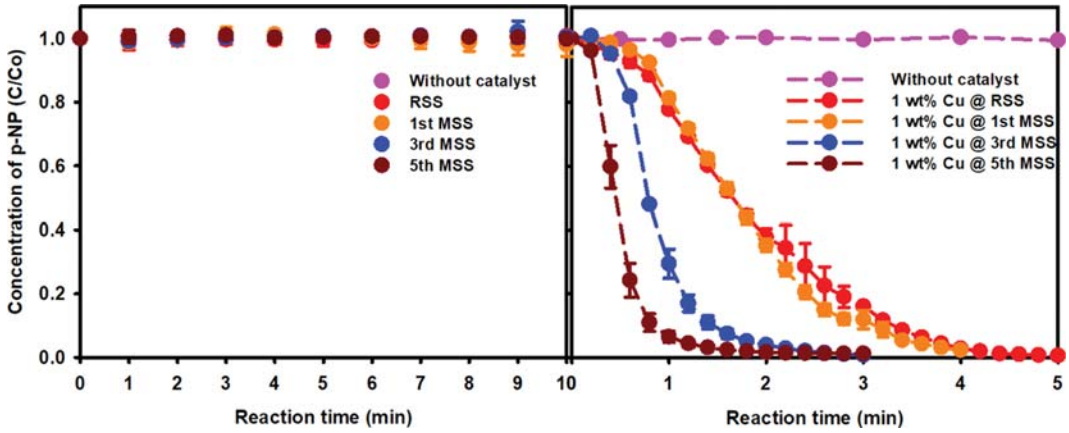

Fig. 9. (a) Concentration change of *p*-NP by different support materials (RSS, 1st-MSS, 3rd-MSS, and 5th-MSS) and (b) after 1 wt% Cu loadings. Experimental conditions: [Catalyst]=2 g/L, [$NaBH_4$]=50 mM, and [*p*-NP]=0.1 mM.

relatively long time (i.e., 60 min) because of the increase in the pH arising from the dissolution of Ca species (e.g., CaO and $Ca(OH)_2$) in the MSS. However, no decrease in the peak intensity at 400 nm was observed, indicating the adsorption and reduction of *p*-NP did not occur in the absence of $NaBH_4$. In contrast, Cu@MSS with $NaBH_4$ showed a continuous decrease in the intensity of the peak at 400 nm over 3 min and an increase in a new peak at 300 nm (Fig. 8(c)) that corresponds to *p*-AP [18,19,23,27,39,40]. Furthermore, a color change from yellow (*p*-nitrophenolate ion) to colorless (*p*-AP) occurred within 3 min, and the used Cu@MSS was easily collected by a magnet (Fig. 8(d)). The results from surface analysis and catalysis experiments indicate that Cu on the MSS surface can be reduced to Cu(0) by $NaBH_4$, and subsequently, the catalytic reduction of *p*-NP with $NaBH_4$ can proceed.

We evaluated the catalytic activity of different Cu@MSSs prepared by using MSSs with different number of separations (RSS, 1st MSS, 3rd MSS, and 5th MSS). Control test using $NaBH_4$ solution (50 mM) without any catalyst material showed no reduction of *p*-NP (Fig. 9). Also, different MSSs without Cu loading were used to identify any catalytic activity of the supports alone (Fig. 9(a)), but there were no significant changes over 10 min. This indicates that adsorption of *p*-NP on the MSSs surface was negligible, even

in the presence of $NaBH_4$. On the other hand, the *p*-NP concentration decreased drastically in 5 min in the suspension of 1 wt% Cu@MSS (Fig. 9(b)). Interestingly, the efficiency of *p*-NP reduction by Cu@MSS was enhanced as the number of magnetic separation pretreatments increased (Cu@MSS (5^{th})>Cu@MSS (3^{rd})> Cu@MSS (1^{st})). This may be caused by the sequential and cumulative removal of $Ca(OH)_2$, which is a known inhibitor of catalytic *p*-NP reduction, from the MSS surface [18]. Note that Cu nanoparticles can show a synergistic effect on *p*-NP reduction with $NaBH_4$ in the presence of iron oxides [25]. Our experimental results and the results of other studies indicate that the high and low contents of Fe_2O_3 and CaO, respectively, in 5^{th}-MSS can lead to enhanced *p*-NP reduction owing to the synergistic effect of Cu and Fe and removal of the inhibitor (i.e., Ca species). Based on the results, we selected the 5^{th}-MSS as a support material for the Cu@MSS catalyst for further studies.

4. Effects of Experimental Factors on the Catalytic Activity of Cu@MSS

To investigate the effect of various experimental factors such as the Cu loading, catalyst concentration, and $NaBH_4$ concentration, further experiments were conducted where each experimental parameter was varied. The *p*-NP reduction kinetics are described by pseudo-first-order kinetics:

$$\ln(A_t/A_0)=\ln(C_t/C_0)=-k_{obs\text{-}pNP}\,(t-t_0), \quad (3)$$

where A is the absorbance at 400 nm of UV-vis spectra, C is the reactant concentration, $k_{obs\text{-}pNP}$ is the observed pseudo-first-order rate constant (min^{-1}), and t_0 is the induction time. We calculated the rate constant by excluding the induction time where *p*-NP was not reduced [25,41]. The induction time excluded at each condition is shown in Table 2.

Table 2. Induction time at different reaction conditions

Reaction condition	Cu loading	Catalyst loading	$NaBH_4$ concentration	Induction time
Effect of Cu loading (Fig. 10)	0.25 wt%	6 mg (2 g/L)	50 mM	120 s
	0.5 wt%	6 mg (2 g/L)	50 mM	60 s
	0.75 wt%	6 mg (2 g/L)	50 mM	30 s
	1 wt%	6 mg (2 g/L)	50 mM	12 s
	1.5 wt%	6 mg (2 g/L)	50 mM	12 s
Effect of catalyst loading (Fig. 12)	1 wt%	3 mg (1 g/L)	50 mM	24 s
	1 wt%	4 mg (1.33 g/L)	50 mM	24 s
	1 wt%	5 mg (1.66 g/L)	50 mM	24 s
	1 wt%	6 mg (2 g/L)	50 mM	12 s
	1 wt%	8 mg (2.66 g/L)	50 mM	12 s
	1 wt%	10 mg (3.33 g/L)	50 mM	12 s
Effect of NaBH4 concentration (Fig. 13)	1 wt%	6 mg (2 g/L)	10 mM	12 s
	1 wt%	6 mg (2 g/L)	25 mM	12 s
	1 wt%	6 mg (2 g/L)	50 mM	12 s
	1 wt%	6 mg (2 g/L)	75 mM	12 s
	1 wt%	6 mg (2 g/L)	100 mM	12 s

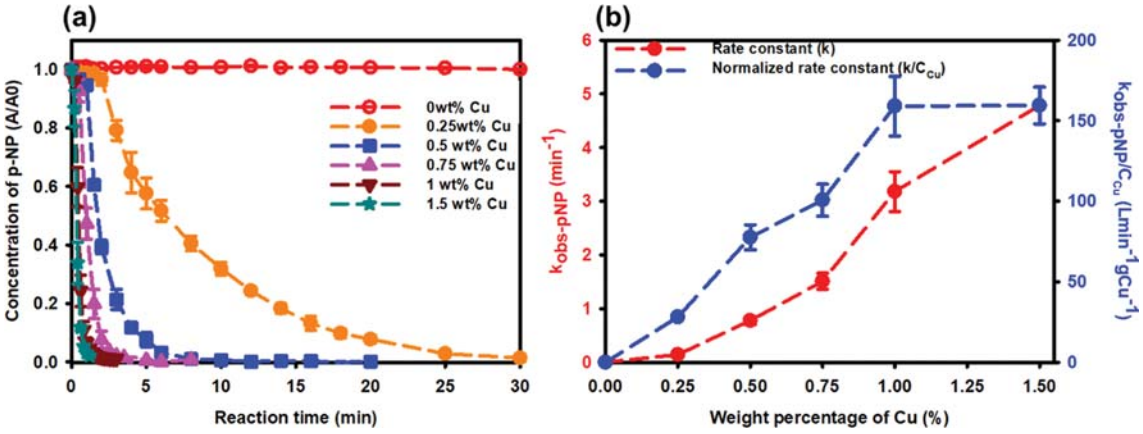

Fig. 10. (a) Catalytic reduction of *p*-NP by Cu@MSS at different Cu loadings (0, 0.25, 0.5, 0.75, 1, and 1.5 wt%) and (b) variation of rate constant and normalized rate constant at each condition. Experimental conditions: [Catalyst]=2 g/L, [$NaBH_4$]=50 mM, and [*p*-NP]= 0.1 mM.

4-1. Effect of Cu Loading

Fig. 10 shows the effect of Cu loading on the catalytic *p*-NP reduction. We prepared five different Cu@MSS catalysts with different Cu loadings (0.25, 0.5, 0.75, 1.0, and 1.5 wt%). Compared to 0 wt%, Cu@MSS showed no significant *p*-NP reduction and almost complete reduction of *p*-NP was observed within 30 min for the 0.25 wt% Cu@MSS (Fig. 10(a)). The increase in Cu loading led to a gradual increase in the $k_{obs\text{-}pNP}$ value (Fig. 10(b)) up to 1.5 wt% (4.78 min^{-1}), indicating that increasing the Cu loading can increase the reactive surface area [42]. It has been reported that excessive metal loading can inhibit the reduction kinetics of *p*-NP because the metal can pile up and can even form aggregate particles, thus blocking active sites [19]. However, no inhibition of *p*-NP reduction was observed with increase in Cu loading, indicating that the Cu nanoparticles were well dispersed on the MSS surface without the severe aggregation of particles until the highest Cu loading examined in this study (i.e., 1.5 wt%).

The $k_{obs\text{-}pNP}$ values were normalized by the Cu concentration (C_{Cu}) to obtain the $k_{obs\text{-}pNP}/C_{cu}$ values (Fig. 10(b)). $k_{obs\text{-}pNP}/C_{cu}$ increased continuously until 1 wt% Cu@MSS (159 L $min^{-1}g_{cu}^{-1}$) and reached a constant level. It is well known that $k_{obs\text{-}pNP}$ is strictly proportional to the total number of active site of metal particles [43], which indicates that the $k_{obs\text{-}pNP}/C_{Cu}$ should be constant with increasing the Cu loading. However, our results are not consistent with this rule, indicating that our support material (i.e., Fe in MSS) could work as a co-catalyst with the Cu nanoparticles, resulting in synergistic *p*-NP reduction. For this reason, Cu@MSS showed 2-400 times higher values for $k_{obs\text{-}pNP}/C_{Cu}$ than other previously reported Cu catalysts without support material (Table 3) [44-46], suggesting that MSS support could improve the catalytic activity of Cu catalyst. To identify the oxidation states of Fe on the Cu@MSS surface before activation, after activation by $NaBH_4$, and after reaction with 0.1 mM *p*-NP, we performed additional XPS analysis (Fig. 11). The peak shifts of the $Fe(2p_{1/2})$ and $Fe(2p_{3/2})$ were not observed after the activation, but the Fe(III) satellite peak decreased significantly after the activation by $NaBH_4$. Then, the Fe(III) satellite was re-formed after the reduction of 0.1 mM *p*-NP, indicating that changes of Fe oxidation state on the Cu@MSS surface during the reaction. After Cu@MSS was transferred to the $NaBH_4$ solution, non-active Fe(III) sites on the MSS surface were reduced by

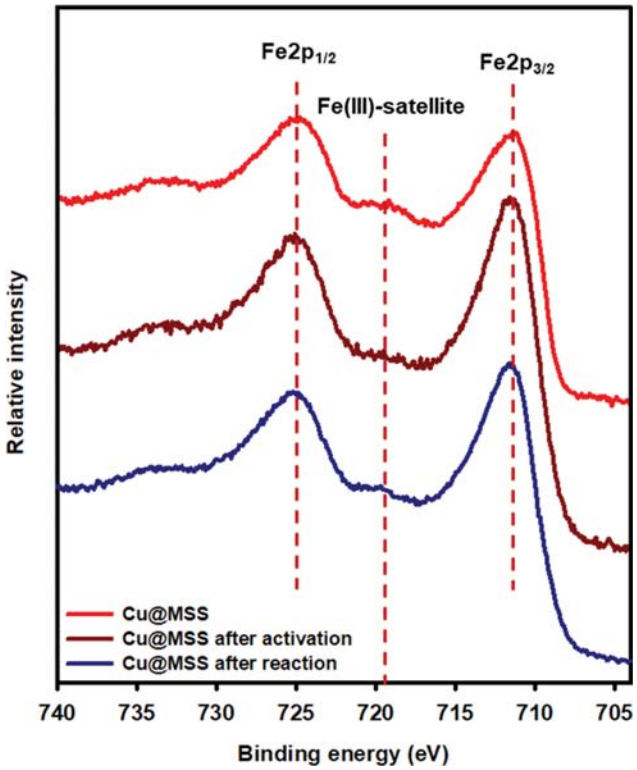

Fig. 11. XPS spectra for the narrow scan of Fe(2p) on the surface of 1 wt% Cu@MSS, after the activation by $NaBH_4$, and after the reaction with *p*-NP. Experimental conditions: [Catalyst]= 2 g/L, [$NaBH_4$]=50 mM, and [*p*-NP]=0.1 mM.

$NaBH_4$ [18] and the newly formed Fe(0) or Fe(II) sites could donate the electron to the Cu nanoparticles [25], resulting in the enhanced activation of Cu nanoparticles.

Although the synergistic effect between Cu and Fe may increase the $k_{obs\text{-}pNP}/C_{cu}$ up to 1 wt% of Cu loading, at higher Cu loadings, the synergistic effect could be reduced because of the excessive amount of Cu, which may cover the Fe sites. Thus, in this situation, $k_{obs\text{-}pNP}$ can only be increased by increasing Cu content but not via the Fe synergistic effect, and the $k_{obs\text{-}pNP}/C_{cu}$ reaches a steady state as shown in Fig. 10(b).

Table 3. Comparison of rate constant ($k_{obs\text{-}pNP}$) and normalized rate constant ($k_{obs\text{-}pNP}/C_{Cu}$) of Cu@MSS with other Cu catalysts for *p*-NP reduction

Catalyst	*p*-NP (mM)	Cu (g/L)	$NaBH_4$ (mM)	$k_{obs\text{-}pNP}$ (min^{-1})	$k_{obs\text{-}pNP}/C_{Cu}$ ($Lmin^{-1}gCu^{-1}$)	Ref.
9.5 nm Cu cubes	0.068	0.038	11.2	0.606	15.95	44
18.0 nm Cu polyhedron	0.068	0.038	11.2	0.342	9	44
21.5 nm Cu polyhedron	0.068	0.038	11.2	0.246	6.47	44
Porous Cu microsphere	0.16	0.016	10	0.246	15.375	45
Solid Cu microsphere	0.16	0.016	10	0.084	5.25	45
Cu nanobranches	0.16	0.016	10	0.126	7.875	45
Cu spheroid	0.1	0.33	10	0.1130	0.342	46
Cu_2O	0.1	0.33	10	0.0527	0.159	46
CuO	0.1	0.33	10	0.0257	0.077	46
1 wt% Cu@MSS	0.1	0.02	10	0.6191	30.9	This work

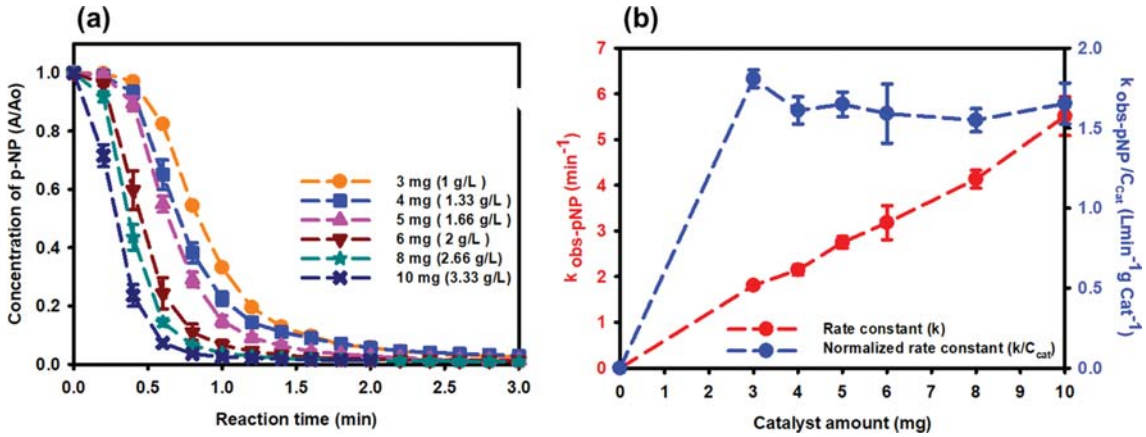

Fig. 12. (a) Catalytic reduction of *p*-NP by 1 wt% Cu@MSS at different catalyst loadings (1, 1.33, 1.66, 2, 2.66, and 3 g/L) and (b) variation of rate constant and normalized rate constant at each condition. Experimental conditions: [$NaBH_4$]=50 mM, and [*p*-NP]=0.1 mM.

4-2. Effect of Catalyst Loading

Fig. 12 shows the effect of catalyst concentration (1, 1.33, 1.66, 2, 2.66, and 3.33 g/L) on the *p*-NP reduction by the 1 wt% Cu@MSS catalyst. Under all conditions, the complete reduction of *p*-NP was observed within 3 min (Fig. 12(a)). A nearly linear relationship was observed between the catalyst loading and $k_{obs\text{-}pNP}$, as shown in Fig. 12(b), indicating that the number of active sites available for the catalytic reduction of *p*-NP increased with increasing catalyst loading. However, the rate constant normalized by the amount of catalyst ($k_{obs\text{-}pNP}/C_{catalyst}$) did not show an increasing trend, indicating that a large amount of Cu@MSS is not required when the catalytic reaction must be finished within a few minutes (<3 min). However, we observed a variation of induction time during the catalyst loading experiments, which is the initial period of *p*-NP adsorption on the active site or the surface restructuring time before catalytic reaction [47], and 2 g/L of Cu@MSS loading showed the lowest induction time (Table 2).

4-3. Effect of $NaBH_4$ Concentration

Fig. 13(a) shows the reduction kinetics of *p*-NP by 1 wt% Cu@MSS in different $NaBH_4$ solutions (10, 25, 20, 75, and 100 mM). It was observed that *p*-NP was converted to *p*-AP almost completely within 5 min at all $NaBH_4$ concentrations. The removal efficiency and the $k_{obs\text{-}pNP}$ values were significantly enhanced with increasing $NaBH_4$ concentration (Fig. 13(b)). Furthermore, the *p*-NP reduction kinetics in the presence of Cu@MSS followed the pseudo-first-order kinetic model, as generally observed in this study, except at 10 mM $NaBH_4$ concentration, which followed the zero-order-kinetic model. This may be because the concentration of $NaBH_4$ (10 mM) may not be sufficient to induce a first-order reaction [43]. Fig. 13(b) also shows the rate constant normalized by the $NaBH_4$ concentration ($k_{obs\text{-}pNP}/C_{NaBH4}$), which revealed the highest value at 25 mM $NaBH_4$. This result indicates that 25 mM $NaBH_4$ could be the optimal concentration for efficient reduction of *p*-NP by Cu@MSS. At high $NaBH_4$ concentration (>25 mM), Cu@MSS can react with $NaBH_4$ aggressively, resulting in excessive production of hydrogen bubbles during the reaction (inset of Fig. 13(b)). This interferes with *p*-NP reduction on the active surface of Cu@MSS [19,20,25].

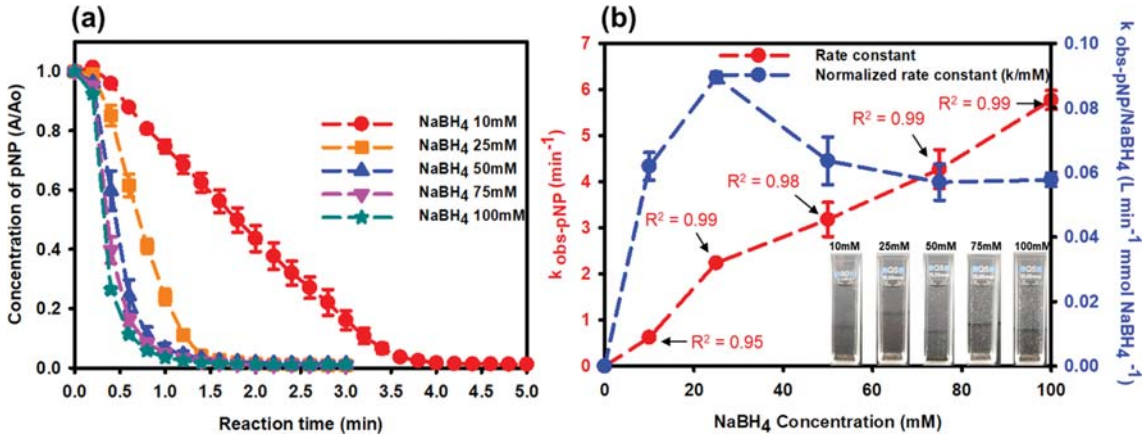

Fig. 13. (a) Catalytic reduction of *p*-NP by 1 wt% Cu@MSS at different concentrations of $NaBH_4$ (10, 25, 50, 75, and 100 mM) and (b) variation of rate constant and normalized rate constant at each condition. Experimental conditions: [Catalyst]=2 g/L, and [*p*-NP]= 0.1 mM.

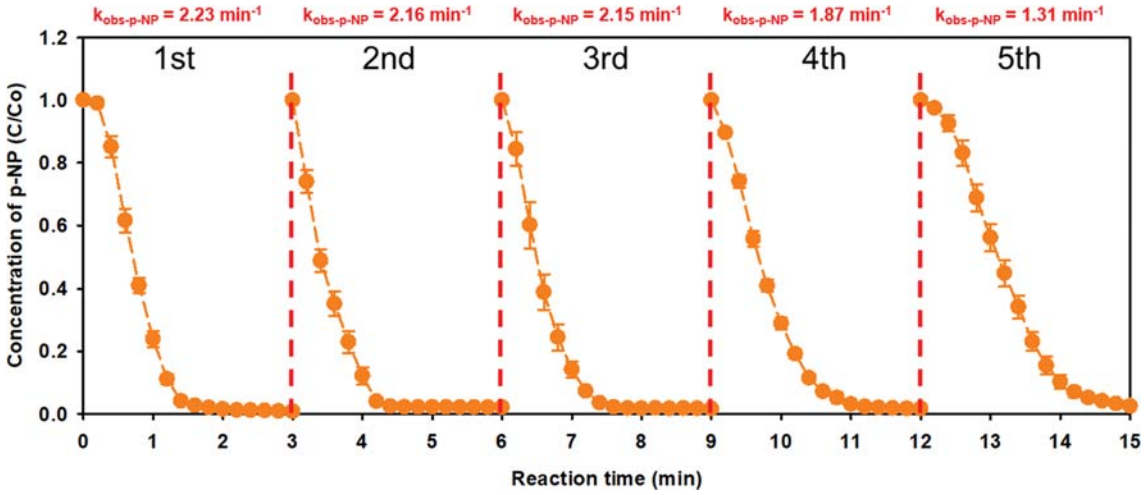

Fig. 14. Reduction kinetics of *p*-NP (0.1 mM) by 1 wt% Cu@MSS (2 g/L) in the presence of $NaBH_4$ (25 mM) during the recycling test.

5. Recycling of the Cu@MSS Catalyst

We investigated the stability and recyclability of 1 wt% Cu@MSS catalysts (2 g/L) by conducting five recycling tests for catalytic *p*-NP reduction (0.1 mM) with 25 mM $NaBH_4$ (Fig. 14). The catalyst used at each cycle was easily collected by magnetic separation after finishing the catalytic reduction of *p*-NP. We observed almost complete reduction of *p*-NP within 3 min in all five cycles, indicating the good reusability and stability of Cu@MSS during the successive reactions. However, the $k_{obs\text{-}pNP}$ values decreased slightly as each cycle proceeded (from 2.23 min^{-1} in the 1st cycle to 1.31 min^{-1} in the 5th cycle). The decrease in the reaction kinetics could be caused by a small loss of catalyst during the washing process. Because we performed small batch-scale reactions in the quartz cuvette, even the loss of a small amount of catalyst could significantly affect the reaction kinetics in the recycling tests [19,20,27].

CONCLUSION

The need for recycling methods to convert solid waste into value-added materials has increased because of environmental and economic concerns. In this study, we successfully developed a recyclable and reactive Cu catalyst using pretreated SS (i.e., MSS). A pretreatment step using the magnetic separation of SS with water was carried out up to five times, resulting in significant increases in the Fe content and decrease in the Ca, a known catalysis inhibitor, content of the MSS. The increased Fe content and removal of Ca species accelerated the reduction kinetics of *p*-NP because Fe acts as a co-catalyst with the doped Cu nanoparticles and the inhibitory effect of Ca was removed. Parametric studies showed that Cu concentration, catalyst amount, and $NaBH_4$ concentration can influence the catalytic *p*-NP reduction significantly. Recycling tests of Cu@MSS revealed its good stability and reusability over five repeated catalytic cycles. The experimental results obtained from this study show the excellent potential of MSS as a support material for the synthesis of novel metallic catalysts, which can be applied to various environmental and industrial clean-up processes.

ACKNOWLEDGEMENTS

We acknowledge the support of the National Research Foundation of Korea (project nos. NRF-2019R1C1C1003316) and the Korea Institute of Energy Technology Evaluation and Planning (KETEP) and the Ministry of Trade, Industry and Energy (MOTIE, 20174010201490).

REFERENCES

1. S. M. Kassim, *Macromol. Symp.*, **320**, 43 (2012).
2. J. Kim, H. S. Kim and S. Bae, *Membr. Water Treat.*, **10**, 1 (2019).
3. S. Yoon and S. Bae, *J. Hazard. Mater.*, **365**, 751 (2019).
4. H. Alanyali, M. Çöl, M. Yilmaz and Ş. Karagöz, *Waste Manag.*, **26**, 1133 (2006).
5. P. E. Tsakiridis, G. D. Papadimitriou, S. Tsivilis and C. Koroneos, *J. Hazard. Mater.*, **152**, 805 (2008).
6. S. Hamid, S. Bae and W. Lee, *Chem. Eng. J.*, **348**, 877 (2018).
7. L. V. Fisher and A. R. Barron, *Resour. Conserv. Recycl.*, **146**, 244 (2019).
8. T. Zhang, Q. Yu, J. Wei, J. Li and P. Zhang, *Resour. Conserv. Recycl.*, **56**, 48 (2011).
9. J.-Y. Lee, J.-S. Choi, T.-F. Yuan, Y.-S. Yoon and D. Mitchell, *Materials (Basel)*, **12**, 1371 (2019).
10. W. J. J. Huijgen, G. J. Witkamp and R. N. J. Comans, *Environ. Sci. Technol.*, **39**, 9676 (2005).
11. X. Wang and Q. S. Cai, *Pedosphere*, **16**, 519 (2006).
12. H. Y. Poh, G. S. Ghataora and N. Ghazireh, *J. Mater. Civ. Eng.*, **18**, 229 (2006).
13. E. Repo, J. K. Warchoł, L. J. Westholm and M. Sillanpää, *J. Ind. Eng. Chem.*, **27**, 115 (2015).
14. Y. J. Zhang, L. C. Liu, Y. Xu, Y. C. Wang and D. L. Xu, *J. Hazard. Mater.*, **209-210**, 146 (2012).
15. M. Cheng, G. Zeng, D. Huang, C. Lai, Y. Liu, P. Xu, C. Zhang, J. Wan, L. Hu, W. Xiong and C. Zhou, *Chem. Eng. J.*, **327**, 686 (2017).
16. K. Horii, T. Kato, K. Sugahara, N. Tsutsumi and Y. Kitano, *Nippon Steel Sumitomo Met. Tech. Rep.*, 109 (2015).

17. J. Zhao, D. Wang, P. Yan and W. Li, *Appl. Sci.*, **6**, 237 (2016).
18. J. Park and S. Bae, *Chemosphere*, **202**, 733 (2018).
19. M. Kim and S. Bae, *Chemosphere*, **212**, 1020 (2018).
20. J. Park and S. Bae, *J. Hazard. Mater.*, **371**, 72 (2019).
21. Y. S. Chan, M. K. Chan, S. K. Ngien, S. Y. Chew and Y. K. Teng, *Membr. Water Treat.*, **9**, 1 (2018).
22. S. Khosroyar and A. Arastehnodeh, *Membr. Water Treat.*, **9**, 481 (2018).
23. X. Du, J. He, J. Zhu, L. Sun and S. An, *Appl. Surf. Sci.*, **258**, 2717 (2012).
24. J. Jung, S. Bae and W. Lee, *Appl. Catal. B Environ.*, **127**, 148 (2012).
25. J. Park and S. Bae, Presented at the 2nd international conference on Bioresources, Energy, Environment, and Materials Technology (BEEM 2018), Hongcheon, Korea, June 10-13, 2018.
26. T. R. Mandlimath and B. Gopal, *J. Mol. Catal. A Chem.*, **350**, 9 (2011).
27. S. Bae, S. Gim, H. Kim and K. Hanna, *Appl. Catal. B Environ.*, **182**, 541 (2016).
28. J. Kim and S. Bae, *Environ. Eng. Res.*, **24**, 646 (2019).
29. Z. Xi, Z. Jingdong, W. Shengzhe and L. Fei, *Open Chem.*, **16**, 583 (2018).
30. X. Lin, X. Lv, L. Wang, F. Zhang and L. Duan, *Mater. Res. Bull.*, **48**, 2511 (2013).
31. S. Pu and M. Liu, *J. Alloys Compd.*, **481**, 851 (2009).
32. S. Jung, S. Bae and W. Lee, *Environ. Sci. Technol.*, **48**, 9651 (2014).
33. L. Feng, R. Wang, Y. Zhang, S. Ji, Y. Chuan, W. Zhang, B. Liu, C. Yuan and C. Du, *J. Mater. Sci.*, **54**, 1520 (2019).
34. H. Hadj Mokhtar, B. Boukoussa, R. Hamacha, A. Bengueddach and D. El Abed, *RSC Adv.*, **5**, 93438 (2015).
35. W. Luo, R. Jin, Y. Qin, F. Huang and C. Wang, *Appl. Phys. Res.*, **2**, 156 (2010).
36. M. Chen, H. Zhu, X. Li, J. Yu, H. Cai, X. Quan, K. Wang and J. Zhang, *J. Nanomater.*, **2014**, 1 (2014).
37. Z. Baolin, G. Qi, H. Xueliang, W. Shurong, Z. Shoumin, W. Shihua and H. Weiping, *J. Mol. Catal. A Chem.*, **249**, 211 (2006).
38. Q. Feng, W. Zhao and S. Wen, *J. Alloys Compd.*, **744**, 301 (2018).
39. S. Pandey and S. B. Mishra, *Carbohydr. Polym.*, **113**, 525 (2014).
40. A. Bhattacharjee and M. Ahmaruzzaman, *RSC Adv.*, **6**, 41348 (2016).
41. S. Gu, Y. Lu, J. Kaiser, M. Albrecht and M. Ballauff, *Phys. Chem. Chem. Phys.*, **17**, 28137 (2015).
42. S. Arora, P. Kapoor and M. L. Singla, *React. Kinet. Mech. Catal.*, **99**, 157 (2010).
43. S. Wunder, F. Polzer, Y. Lu, Y. Mei and M. Ballauff, *J. Phys. Chem. C.*, **114**, 8814 (2010).
44. P. Zhang, Y. Sui, G. Xiao, Y. Wang, C. Wang, B. Liu, G. Zou and B. Zou, *J. Mater. Chem. A.*, **1**, 1632 (2013).
45. M. Li, Y. Su, J. Hu, H. Geng, H. Wei, Z. Yang and Y. Zhang, *Mater. Res. Bull.*, **83**, 329 (2016).
46. S. Ghosh, R. Das, I. H. Chowdhury, P. Bhanja and M. K. Naskar, *RSC Adv.*, **5**, 101519 (2015).
47. S. Bae, S. Gim, H. Kim, V. Dorcet, M. Pasturel, J. M. Grenèche, G. K. Darbha and K. Hanna, *J. Phys. Chem. C.*, **121**, 25195 (2017).